# A quantitative study of the influence of soil organic carbon and pore characteristics on the stability of aggregates of the karst peak-cluster depression area in Southwest China

Hui Wei[1] · Yusong Deng[1,2] · Juan Huang[1] · Ling He[1] · Qiuyue Tang[1] · Yan Xiao[1]

## Abstract

**Purpose** Rock desertification is the most serious ecological problem in karst areas and can easily cause soil structure instability. The aim of this work was to analyze the influences of organic carbon, carbon components and pore structural differences on the stability of aggregates in rocky desertification areas.

**Materials and methods** Soil samples were collected from the karst peak-cluster depression area in Southwest China. Soil aggregate stability was determined by the Le Bissonnais (LB) method. The relationship between variables was analyzed via the structural equation model (SEM).

**Results and discussion** There were significant differences in the stability of aggregates among different land uses in the study area: secondary forest (SF) > coppice forest (CF) > plantation forest (PF) > citrus plantation (CP) > cultivated land (CL). The main crushing mechanisms of aggregates were slaking and mechanical failure. Aggregate pores were mainly < 30 μm storage pores, with pore throat diameters concentrated in the 0–20 μm range, which was associated with the cohesive soil texture of the study area. The pore connectivity of aggregates was better in SF and CF, followed by PF, while CP and CL had lower colloidal material contents, isolated pore structure and poor connectivity due to the heavy application of inorganic fertilizers and influences from human disturbances.

**Conclusions** SEM analysis showed that SOC and POC determined aggregate stability, mainly by directly or indirectly influencing aggregate porosity and the number of storage pores. The POC was the main variable in organic carbon composition to determine the pore characteristics and stability of aggregates. To meet the bidirectional demand of production and improvement of soil structure, it is necessary to rationally distribute fertilizer and reduce disturbance frequency in agricultural production land.

**Keywords** The peak-cluster depression area · Aggregate pore · Soil organic carbon · Computed tomography (CT) scan · Aggregate stability

✉ Yusong Deng
denny2018@gxu.edu.cn

1  Forestry College of Guangxi University, No. 100 Daxue Road, Nanning 530004, China

2  Huanjiang Observation and Research Station for Karst Ecosystems, Chinese Academy of Sciences, Huanjiang 547100, Guangxi Province, China

## 1 Introduction

The karst region of Southwest China is the core distribution area with the strongest karstification and the largest area in the world (Sweeting 1973; Liu et al. 2016). The peak-cluster depression area is one of the comprehensive control areas of karst rocky desertification. Due to the unique karst pore structure (Kan et al. 2020), it causes serious water and soil loss, shallow soil layer and weak anti-interference ability which is a typical ecological fragile area (White and White 2005). Fully understanding the karst soil structure and properties is key to controlling the development of rocky

desertification and breaking the shackles that restrict the local realization of sustainable development.

The aggregate is a basic unit of the soil structure (Mikha and Rice 2004); a product of the interaction of mineral particles with cementitious materials (Edwards and Bremner 1967; Tisdall and Oades 1982) and its characteristics is an important reference for soil quality (Bronick and Lal 2005). Organic carbon, as an important cementing substance in soils, impacts the structural characteristics and stability of aggregates in multiple ways (Sarker et al. 2018). However, current studies on soil structure are mostly limited to the number, distribution and stability of aggregates while ignoring essential characteristics of soil structure, particularly pore structure (Six and Paustian 2014; Ma et al. 2020; Wu et al. 2021). The pore structure as an important soil property (Jozefaciuk et al. 2015; Ma et al. 2020) that determines soil solute transport, gas exchange rate and microbial activity (Kravchenko and Guber 2016; Yu et al. 2017; Cássaro et al. 2017). Studies have also shown that the distribution of organic carbon in aggregates is related to their internal pore structure (Larsbo et al. 2016). Pore structure heterogeneity may influence the physical carbon sequestration capacity of soils and even modify microbial activity and distribution to facilitate or inhibit decomposition of soil organic carbon (Nunan et al. 2006; Kravchenko et al. 2015). The pore structure as well as an important variable controlling the stability of aggregates (Yu et al. 2017, 2018) which together with the soil particle composition and its cementing material determines the aggregation capacity and slaking potential of the aggregates (Barral et al. 1998; Papadopoulos et al. 2009). Dal Ferro et al. (2012a, b) also proposed that soil porosity is significantly related to aggregate stability. In addition, a well-structured pore can provide abundant attachment sites for mycelial growth (Kravchenko et al. 2015; Ananyeva et al. 2013) and solidifying the aggregate structure. Therefore, there must be a significant link between organic carbon in the aggregates and the soil pore structure and aggregate stability.

In recent years, pore characteristics have been used to characterize the structural quality of soils. However, direct access to the internal structure of soils, especially the microstructure at the aggregate scale, has remained challenging because of the complexity of soil constituents and the structural fragility of aggregates (Garbout et al. 2013a). The visualization and quantitative analysis of aggregate pore structure is a major challenge in soil science research (Pagliai et al. 2004; Deurer et al. 2009; Yang et al. 2014; Guo et al. 2020). As a nondestructive and efficient measurement technique that provides high-definition images rapidly and at extremely high separation rates, CT scanning is considered an effective means of studying aggregate pores (Ferro et al. 2013; Garbout et al. 2013b; Zhang et al. 2016; Pires et al. 2020; Zhao et al. 2020). It can be combined with various image processing technologies to obtain the pore space form, and it can be used to perform quantitative calculations to obtain pore parameters such as the porosity, pore number, equivalent diameters of aggregate pores and rates of reactions occurring within complex pores (Cercioglu et al. 2018; Wang et al. 2019; Feng et al. 2019, 2020). The feasibility of this approach has been verified.

Previous studies have found that soil pore characteristics are influenced by multiple factors, including land use, land management practices and soil type (Zhou et al. 2012; Costa et al. 2014; Feng et al. 2019; Yu et al. 2019). Researchers have also studied the effect of cementing substances on the microstructure of aggregates (Gargiulo et al. 2013; Regelink et al. 2015; Yu et al. 2017). However, minimal research has explored the extent to which cementing substances affect the pore structure of aggregates and quantified the main relationship between cementing substances and aggregate stability.

Considering that soil is at the link and core part of the material cycle and shows an extremely sensitive environmental response. At the same time, due to the fragile ecological environment of the study area, the increase in severe rocky desertification and the decline or even loss of land productivity, economic and land conflicts are particularly prominent, while land use has to balance the needs of multiple aspects, making the types very complex. Combined with the nature of karst soils themselves nutrients are highly susceptible to leaching resulting in uneven distribution or deficiency (Fenton et al. 2017; Xiao et al. 2019). It also exhibits sensitivity to anthropogenic disturbances (Barral et al. 1998), while tillage and fertilization can cause fragmentation of the original soil pore structure and rapid decomposition and loss of nutrients including cementing materials (Menon et al. 2015; Zhuo et al. 2016). Therefore, Changes in land-use practices have different degrees of impacts on the microporous structure and cementitious material content of soils, which can ultimately result in differences in the structural stability of lime soils.

In this study, we hypothesized that the organic carbon content of karst soils affects their internal pore structure and causes differences in the stability of aggregates. To test this hypothesis, we evaluated the internal pore structure of the five most commonly encountered land-use aggregates in the study area by CT scanning and quantitatively analyzed the relationships between the variables in conjunction with the structural equation model (SEM). Soil samples were also collected at the longitudinal level to compare the variability between their soil microstructures. The goals of this study were (i) to assess the structural characteristics and main influencing factors of aggregates in the southwestern karst region, (ii) to explore the coupling between organic carbon and the soil microporous structure and (iii) to clarify the mechanisms by which the characteristics of soil organic carbon and pore characteristics contribute to the stability of aggregates.

## 2 Materials and methods

### 2.1 Overview of the study area

The study area is located in Guling Town, Mashan County, Nanning City, Guangxi, China (107°41′-108°29′ E, 23°24′-24°02′ N), a typical karst peak-cluster depression area, the location of which is shown schematically in Fig. 1. The region is in the southern subtropical monsoon climatic zone, with rain and high temperatures during the same period, a mean annual temperature of 21.2 ℃, an average annual frost-free period of 362 days, average annual sunshine hours of 1479.1 h and an average annual rainfall of 1692.5 mm. The spatial and temporal distribution of rainfall is uneven and mostly concentrated during the summer season, with seasonal droughts occurring from time to time. As a result of long-term unreasonable anthropogenic interference, the native forest has been almost eliminated, resulting in a landscape characterized by rocky desertification. The area is dominated by secondary vegetation, predominating in the area, followed by planted forests and crop cultivation communities. The forest coverage of the district is over 90%. The soils are dominantly limestone soils, which are weakly alkaline, have a clayey texture and present in shallow layers. The karst landscape is fully developed and it is one of the areas with the most severe rocky desertification in Southwest China.

### 2.2 Soil sample collection and determination

In May 2021, five types of representative land-use sample sites, secondary forest (SF), coppice forest (CF), plantation forest (PF), citrus plantation (CP) and cultivated land (CL), all of which had soils developed from carbonate, were selected after field surveys. The use history of each sample site is as follows. The CL is still used for maize cultivation, which is grown twice a year and receives artificial fertilization, soil tillage and weeding two to three times each. The CP sample plots were converted from agricultural land to citrus plantations in 2014 and were treated with fertilizer three times a year to meet production needs, with a mid-tillage loosening in winter. The PF sample plots were planted with economic tree species after being fallowed in 2010, and fertilizer treatments were applied once a year during their young age (within 3 years). The CF was fallowed in 2005 and naturally restored to shrubland, and the SF was fallowed in 1999 and naturally restored to secondary forests. The basic details of the sample site are shown in Table 1.

To control the influence of slope position and gradient on the results of the study, three standard 20 m × 20 m sample plots were set up in each field (including upper, middle and lower slopes), with multiple sampling points following an "S" route, with 10–15 soil samples from each site. As rock desertification affects soil degradation primarily within the 10–40 cm soil layer, we collected undisturbed soil

**Fig. 1** Location diagram of the study area
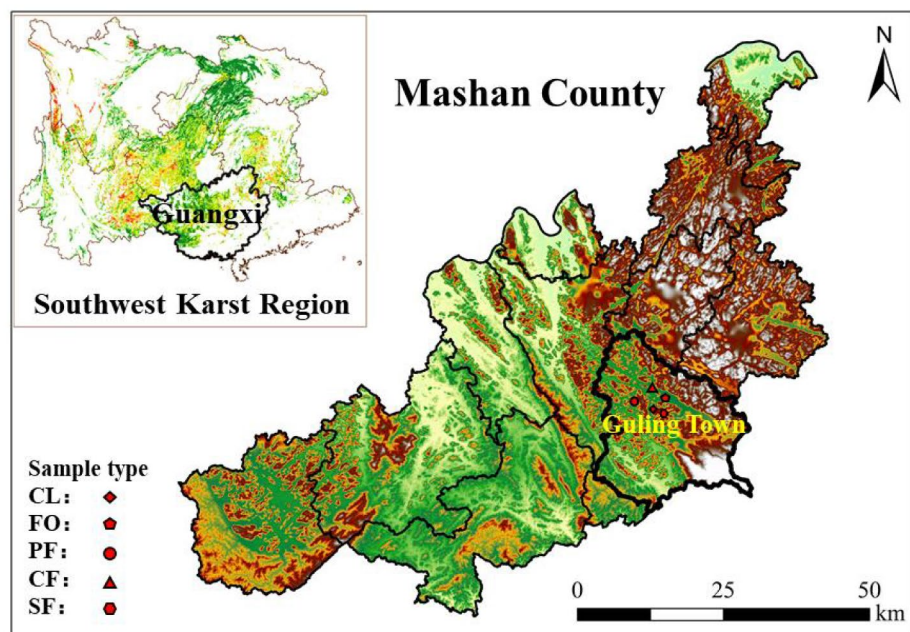


CL cultivated land, CP citrus plantation, PF plantation forest, CF coppice forest, SF secondary forest

**Table 1** Basic information of different land-use sample sites

| Land type | Longitude | Latitude | Altitude/m | Vegetation coverage | Major vegetation types |
|---|---|---|---|---|---|
| CL | 108°31′56″ | 23°62′69″ | 196~200 m | 70%-75% | Maize(*Zea mays*) |
| CP | 108°29′22″ | 23°64′45″ | 213~217 m | 50%-60% | Citrus(*Citrus reticulata Blanco*) |
| PF | 108°27′85″ | 23°64′45″ | 220~233 m | 45%-50% | Chinese toon(*Toona sinensis*)、Winged Podocarpus(*Zenia insignis Chun*)、cogon grass(*Imperata cylindrica*) |
| CF | 108°30′38″ | 23°64′78″ | 233~256 m | 60%-65% | Yellowthorn(*Vitex negundo*)、Kidney Fern(*Nephrolepis auriculata*) |
| SF | 108°29′22″ | 23°64′45″ | 396~402 m | 70%-80% | Yellow basket-willow(*Engelhardtia roxburghiana*)、Aoyamaoka(*Cyclobalanopsis glauca*) |

*CL* cultivated land, *CP* citrus plantation, *PF* plantation forest, *CF* coppice forestmm, *SF* secondary forest

samples and cutting ring soil samples from the 0–20 cm and 20–40 cm soil layers below the soil surface. The undisturbed soils were transported in plastic boxes to prevent damage to the soil structure during transport.

After the soil samples were brought back to the laboratory, debris were removed, and the samples were mixed with the quartering method in the same way. The dried soil was broken into soil blocks of approximately 10 mm along natural cracks. After screening, the stability of aggregates was determined by the Le Bissonnais (LB) method (Le Bissonnais 1996). A portion of the 3–5 mm aggregates was placed in an oven at 40 °C for 24 h and then stored in a refrigerator at 4 °C prior to CT scanning. Another portion of the undisturbed soils was used for the determination of basic physical and chemical properties of the soil by the following methods (Lu 2000): organic carbon by the $H_2SO_4$–$K_2Cr_2O_7$ external heating method; soil bulk density by the cutting ring method; soil water content by the cutting ring dip method; pH by a potentiometric method ($H_2O$, 1:2.5); and soil mechanical composition by a pipette method.

Determination of soil particulate organic carbon (POC) (Garten et al. 1999) was measured as follows. First, 10 g of dry soil was taken through a 2 mm sieve, immersed in 50 ml of $(NaPO_3)_6$ in water, shaken by hand for 15 min and then shaken for 18 h with a shaker (90 r·min$^{-1}$). The soil suspension was sieved through a 53 µm sieve, rinsed several times with distilled water and dried at 60 °C. The residue was weighed, and its proportion of the mass of the soil sample was calculated. The separated POC was determined by external heating with potassium dichromate and then converted to the POC content per unit mass of soil sample. Where mineral organic carbon (MOC) content is equal to total organic carbon content (SOC) minus the particulate organic carbon (POC) content.

The three treatments of LB method are effective in separating the different fragmentation mechanisms of aggregates (Le Bissonnais 1996). Among them, the fast wetting (FW) treatment simulates the slaking process of soil under heavy rainfall or irrigation, the slow wetting (SW) treatment

simulates the slaking of soil aggregates caused by the expansion of soil clay particles under light rain and the prewetted shaking (WS) treatment corresponds to simulating processes such as mechanical tillage fragmentation (Ojeda et al. 2008; Rohosková and Valla 2011).

The following operations were carried out. The screened 3–5 mm aggregate was dried to a constant weight in an oven at 40 °C, and 5 g of the soil sample was weighed and subjected to the following steps. For FW, 5 g of aggregate was quickly immersed in pure water, left for 10 min and excess water was aspirated. For SW, 5 g of aggregate was placed on filter paper, and anhydrous ethanol was slowly added dropwise along the edges until the aggregate was completely immersed and left for 30 min. For WS, 5 g of aggregate was submerged in anhydrous ethanol for 10 min, excess alcohol was drawn off, and the aggregate was transferred to a 250 ml conical flask containing pure water and filled with water to 200 ml, sealed and shaken up and down 20 times at a constant speed and left to stand for 30 min. Then, excess water was removed. Soil samples from each of the three treatments were transferred to different aluminum boxes by using anhydrous ethanol, dried in an oven at 40 °C to a constant weight, sieved and weighed on a 10,000 ppm balance and stability parameters were calculated.

## 2.3 CT scan and image processing

**Image scanning and reconstruction** The aggregate samples were scanned using a Nano Industrial CT (ZEISS Xradia 520). The scanning parameters were set to a voltage of 50 kV and a 60 µA current, with a resolution of 1.2 µm, exposure time of 1 s and a sample stage to detector distance of 1.5 cm. One thousand projection images were taken with the sample stage rotating horizontally from 0 to 360° at a constant speed. CT program software was then used to reconstruct the images, obtaining approximately 800 grayscale images in 32-bit tiff format at 1049×1049 pixels in size using a back-projection algorithm. Then, the images were saved as 8-bit tiff images with a range of gray values from 0 to 255.

**Visualization and analysis of the 3D structure of aggregate pores** (1) The brilliance difference between images was adjusted with the "normalize" command in the Image J software for normalization. (2) To obtain accurate soil structure pore data, the images were noise reduced using median filtering to remove annular artifacts. (3) The region of interest (ROI) of $500 \times 500 \times 500$ voxels in the middle of the aggregate sample was extracted using Image J software to avoid edge effects, which was 1.85 mm $\times$ 1.85 mm $\times$ 1.85 mm in size. (4) The Otus value method (Otus 1979) was used to debug the state of the scanned gray-scale image in combination with the pre-calibrated soil pores to determine the image binary segmentation threshold. Thresholds were set for different soils to maximize the distinction between the soil matrix and pore structure. (5) Image visualization of the 3D structure of aggregate pores was completed by the Image J "3D viewer" plug-in. The quantitative description of the aggregate pore characteristic parameters such as porosity, specific surface area, and number of pore throats was obtained using a "3D suit"; the procedure is shown in Fig. 2.

## 2.4 Calculation formula for parameters

(1) Assessment of the stability parameters of aggregate by the LB method: the mean weight diameter (MWD), relative slaking index (RSI) and relative mechanical index (RMI)

(Le Bissonnais 1996; Zhang and Horn 2001) were calculated as follows.

$$MWD = \sum_{i=1}^{n} \frac{r_{i-1} + r_i}{2} \times m_i \tag{1}$$

In the equation, MWD is the average weight diameter under the 3 different wetting methods of the LB method (FW: fast wetting; SW: slow wetting; WS: pre-wetting shock, respectively), (mm). "$m_i$" indicates the mass percentage of aggregate of the i-th grain size, (%). "r" indicates the average grain size of the two adjacent aggregates (mm). "n" indicates the number of sieves.

$$RSI = \frac{MWD_{SW} - MWD_{FW}}{MWD_{SW}} \times 100\% \tag{2}$$

$$RMI = \frac{MWD_{SW} - MWD_{WS}}{MWD_{SW}} \times 100\% \tag{3}$$

In the equation, $MWD_{FW}$, $MWD_{SW}$ and $MWD_{WS}$ are the MWD values under the 3 treatments of the LB method, respectively (mm). RSI and RMI are the relative slaking index and relative mechanical index, respectively (%).

(2) Calculation of organic carbon and carbon fraction contribution of aggregate.
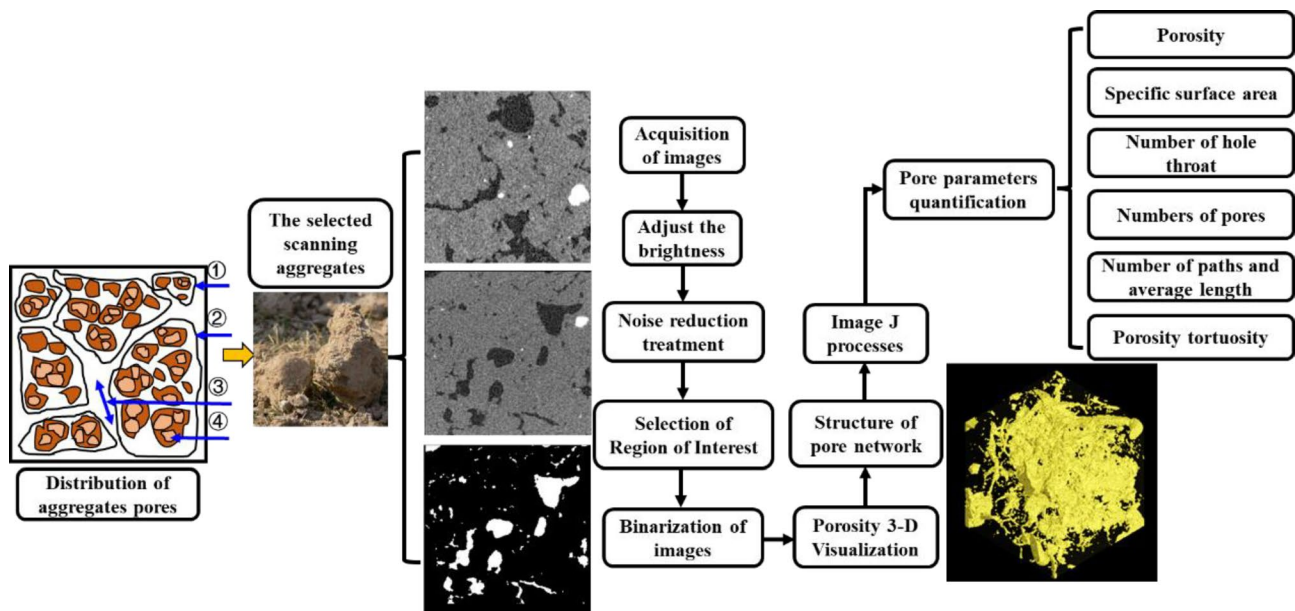


① indicates microaggregate, ② indicates large aggregates, ③ indicates inter-aggregate pores, ④ indicates intra-microaggregate pores

**Fig. 2** Process of visualization and quantitative analysis of aggregate pore images

$$F_{3-5mm} = \frac{ASOC_{3-5mm} \times P_{3-5mm}}{\sum_{i=1}^{6} ASOC_i \times P_{3-5mm}} \times 100\% \qquad (4)$$

In the equation, $F_{3-5}$ mm is the contribution rate of 3–5 mm particle size aggregate, $ASOC_{3-5}$ mm is the total organic carbon or carbon component content of 3–5 mm particle size aggregate, and $P_{3-5}$ mm is the ratio of 3–5 mm particle size aggregate to the total aggregate (%).

## 2.5 Statistics and analysis

The study statistics of this trial were initially collated in Excel, and SPSS 21.0 was used to test the homogeneity of variance of the data. One-way ANOVA was used to analyze the impact of land-use change on soil properties, and LSD method was used for significance multiple comparison (the significance level was set as $P < 0.05$). Origin 21 was used software for plotting.

Structural equation modeling (SEM) was used to evaluate the hypothetical effects of differences in cementitious material between land uses on soil pore structure and aggregate stability, with other variables that directly or indirectly influence these factors. With SEM models built in AMOS 17.0, inspection of model fit was performed using tests including the $\chi^2$ test ($P > 0.05$, CMIN/D.F. < 2), comparative fit index (CFI) (CFI > 0.9), goodness of fit (GFI) (0.8 < GFI < 1), root mean square error of approximation (RMSEM) (< 0.05) and unstandardized residuals RMR (You et al. 2014). The blue and red arrows indicate negative and positive impacts, respectively.

# 3 Results

## 3.1 Basic soil characteristics

Some of the basic properties of the test soils are shown in Table 2. The pH of the soils in the study area was neutral or slightly alkaline, while land-use practices and depth of soil layer had a strong influence on their properties. The soil organic matter (SOM) content varied significantly between land uses, from SF > CF > PF > CP > CL in descending order, with consistent trends between soil layers and a decrease in content with increasing soil profile ($P < 0.05$). The soil bulk density (BD) of the CL site was significantly higher than that of the other sample plots, and those SF and CF were lower and increased with increasing soil depth($P < 0.05$). The oil moisture content in the upper surface layer varied significantly, SF > CF > PF > CP > CL, while in the lower surface layer, the soil moisture content was still the lowest at CL and the highest at SF and decreased with increasing soil depth. However, the soil in the study area was sticky and heavy, and the soil mechanical composition of various places was mainly clay silt, with a low content of sand.

## 3.2 Stability characteristics of aggregates under LB treatment

The mean weight diameter (MWD) values of the aggregate stability parameters under different treatments of the LB method are shown in Table 3: $MWD_{SW} > MWD_{WS} > MWD_{FW}$.

**Table 2** Basic physical and chemical properties of the test soil

| Soil layer | Land type | pH | SOM/(g/kg) | BD/(g/cm³) | SC/(%) | Soil mechanical composition | | |
|---|---|---|---|---|---|---|---|---|
| | | | | | | Sand/(%) | Silt/(%) | Clay/(%) |
| 0–20 cm | CL | 6.64 ± 0.09d | 25.04 ± 0.47e | 1.44 ± 0.04a | 15.84 ± 1.71a | 29.53 ± 0.22a | 37.85 ± 3.83b | 32.61 ± 4.03b |
| | CP | 7.34 ± 0.11c | 29.60 ± 0.32d | 1.31 ± 0.05b | 23.24 ± 4.36a | 27.18 ± 5.24ab | 41.39 ± 4.77b | 31.43 ± 0.87bc |
| | PF | 7.91 ± 0.04ab | 34.71 ± 0.57c | 1.25 ± 0.02bc | 23.73 ± 5.79a | 29.41 ± 6.86a | 42.27 ± 6.40b | 28.33 ± 0.52bc |
| | CF | 7.76 ± 0.04b | 49.64 ± 0.78b | 1.19 ± 0.03c | 26.04 ± 3.14a | 21.77 ± 3.33ab | 43.61 ± 3.25b | 34.62 ± 6.50a |
| | SF | 8.00 ± 0.03a | 63.57 ± 1.11a | 1.21 ± 0.06bc | 26.62 ± 6.28a | 17.29 ± 2.16b | 45.99 ± 3.64a | 36.73 ± 1.80a |
| 20–40 cm | CL | 6.56 ± 0.01d | 14.94 ± 0.47e | 1.45 ± 0.07a | 15.73 ± 4.74b | 23.33 ± 1.36a | 40.23 ± 3.98bc | 36.44 ± 2.96ab |
| | CP | 7.65 ± 0.03c | 21.74 ± 0.23d | 1.29 ± 0.01b | 17.18 ± 3.43ab | 21.67 ± 0.53a | 38.60 ± 3.00c | 39.73 ± 2.47a |
| | PF | 7.94 ± 0.02b | 25.91 ± 0.22c | 1.27 ± 0.02b | 22.07 ± 1.94ab | 21.22 ± 1.75a | 41.30 ± 1.12bc | 37.48 ± 1.36ab |
| | CF | 7.95 ± 0.04b | 31.65 ± 0.13b | 1.24 ± 0.01b | 21.99 ± 5.22ab | 21.58 ± 2.10a | 46.64 ± 3.33ab | 31.78 ± 3.28b |
| | SF | 8.13 ± 0.02a | 48.76 ± 0.75a | 1.24 ± 0.06b | 25.71 ± 2.15a | 12.85 ± 3.55b | 52.31 ± 2.32a | 34.85 ± 1.80ab |

*SOM* soil organic matter, *BD* soil bulk density, *SC* soil moisture content. Significant differences between land-use types are indicated by different lowercase letters in the same column ($P < 0.05$)

**Table 3** Stability parameters of aggregate treated by LB method

| Soil layer | Land type | MWD$_{FW}$/(mm) | MWD$_{SW}$/(mm) | MWD$_{WS}$/(mm) | RSI/(%) | RMI/(%) |
|---|---|---|---|---|---|---|
| 0–20 cm | CL | 1.12±0.01d | 2.92±0.06d | 2.21±0.03d | 61.62±1.10a | 24.22±2.46a |
| | CP | 1.92±0.05c | 3.51±0.05d | 3.07±0.10c | 45.23±2.03b | 12.51±1.77b |
| | PF | 1.97±0.07c | 3.09±0.03c | 2.75±0.15b | 36.26±2.76c | 10.93±5.66bc |
| | CF | 2.47±0.05b | 3.60±0.05ab | 3.37±0.07a | 31.46±1.69d | 6.38±0.67bc |
| | SF | 3.15±0.10a | 3.67±0.02a | 3.52±0.05a | 14.38±2.62e | 4.28±1.83c |
| 20–40 cm | CL | 0.80±0.03d | 2.79±0.05c | 2.03±0.04c | 71.48±1.31ab | 27.18±1.90b |
| | CP | 0.90±0.03d | 3.45±0.06b | 2.89±0.04b | 74.03±1.08a | 16.07±2.34c |
| | PF | 1.13±0.02c | 3.58±0.02a | 2.11±0.13c | 68.35±0.43b | 41.18±3.37a |
| | CF | 2.17±0.11b | 3.54±0.04ab | 3.20±0.08a | 38.57±3.65c | 9.37±3.11d |
| | SF | 2.68±0.04a | 3.61±0.03a | 3.25±0.04a | 25.78±1.75d | 9.93±0.82d |

*MWD$_{FW}$* mean weight diameter for fast wetting treatments, *MWD$_{SW}$* mean weight diameter for slow wetting treatments, *MWD$_{WS}$* mean weight diameter for pre-wetting shaking treatments, *RSI* relative slaking index, *RMI* relative mechanical crushing index

After FW treatment, the MWD value of each land-use aggregate varied from 0.8 mm to 3.15 mm with a coefficient of variation of 42.09%, and the trends of MWD among different soil layers were all SF > CF > PF > CP > CL, with the stability of the aggregates gradually decreasing. Within the 0–20 cm soil layer, there was no significant difference in MWD values between CP and PF, while CL, CF and SF all differed significantly ($P < 0.05$). No significant differences in MWD values were found between CL and CP within the 20–40 cm soil layer, while significant differences were found between PF, CF and SF ($P < 0.05$). The MWD values were relatively high in the SW treatment ranging from 2.79 mm to 3.67 mm. The MWD values for the two soil layers were highest for SF and lowest for CL. There was also variability in MWD values for the same soil layer at different sample sites with a coefficient of variation of 8.93%. The MWD values varied between 2.03 and 3.52 mm with a coefficient of variation of 18.25% under the WS treatment, with the MWD between soil layers yielding the following order: SF > CF > CP > PF > CL. There were no significant differences between the MWD values of CF and SF in the topsoil layer, but both were significantly higher than those of CL, CP and PF ($P < 0.05$). The MWD values were not significantly different between CL and PF or between CF and SF in the lower soil layers, but they were all significantly different from that of CP ($P < 0.05$). All three treatments showed a decrease in MWD values with increasing soil depth. The main fragmentation mechanisms for aggregate slaking in the study area were FW simulating dissipative effects from heavy rainfall or irrigation and WS simulating mechanical damage.

The relative slaking index (RSI) and Relative mechanical index (RMI) measure the sensitivity of aggregates to different damage mechanisms. As shown in Table 3, the RSI values between the two soil layers yielded the order CL > CP > PF > CF > SF, and the difference was significant ($P < 0.05$). The RMI and RSI values showed similar patterns of variation, but the ability of each aggregate to resist dissipation and mechanical damage gradually increased from CL to SF, and the sensitivity to dissipation was stronger than mechanical damage, as shown by the fact that the RMI values were considerably lower than the RSI values.

## 3.3 Characteristics of organic carbon and carbon fraction content and their contribution to aggregates

As shown in Table 4, in the 0–20 cm soil layer, the content of SOC in aggregates of various plots ranged from 14.40 g/kg to 38.47 g/kg, with the order of SF > CF > CP > PF > Cl, with significant differences, and the content contribution rate was 53.67% ~ 78.10% ($P < 0.05$). The distribution of SOC content in the 20–40 cm soil layer ranged from 8.69 g/kg to 32.34 g/kg, with a similar pattern of variation to that of the topsoil layer, with a contribution between 40.45% and 72.85%.

Particulate organic carbon (POC) and mineral organic carbon (MOC) are essential components of organic carbon. As shown in Table 4, the distribution of the MOC content in the aggregate ranged from 7.43 g/kg to 19.00 g/kg. In the 0–20 cm soil layer, the MOC content of CF aggregate was significantly higher than that of other aggregates, with no significant difference between CP and PF, both of which had significantly higher values than CL and SF ($P < 0.05$). The 20–40 cm soil layer featured the order of CP > PF > CF > SF > CL. The content of POC in aggregates varied from 0.79 g/kg to 26.18 g/kg, with significantly higher POC content in the intersoil SF aggregates than in the other aggregates. The content was next highest in the CF aggregates and lower in the CL and CP aggregates. The content of both POC and MOC decreased with

**Table 4** SOC and carbon component content and contribution rate in aggregate

| Soil layer | Land type | SOC /(g/kg) | Contribution rate/(%) | MOC /(g/kg) | Contribution rate/(%) | POC /(g/kg) | Contribution rate/(%) |
|---|---|---|---|---|---|---|---|
| 0–20 cm | CL | 14.40 ± 0.31e | 53.67 ± 0.82e | 11.18 ± 0.83d | 51.99 ± 2.07c | 3.22 ± 0.62d | 45.63 ± 5.43b |
| | CP | 20.23 ± 0.20c | 68.51 ± 0.17d | 14.38 ± 1.54b | 72.84 ± 2.62b | 5.85 ± 1.51c | 51.64 ± 7.91b |
| | PF | 19.28 ± 0.10d | 73.37 ± 0.26c | 14.02 ± 0.29bc | 71.99 ± 0.92b | 5.25 ± 0.31c | 66.54 ± 1.18a |
| | CF | 33.47 ± 0.23b | 76.56 ± 0.12b | 19.00 ± 0.55a | 80.80 ± 0.44a | 14.47 ± 0.40b | 67.03 ± 0.55a |
| | SF | 38.47 ± 0.19a | 78.10 ± 0.07a | 12.29 ± 0.60 cd | 79.02 ± 0.11a | 26.18 ± 0.54a | 74.81 ± 0.15a |
| 20–40 cm | CL | 8.69 ± 0.27d | 40.45 ± 0.47d | 7.43 ± 0.12e | 38.54 ± 1.86c | 1.26 ± 0.15d | 35.20 ± 6.76c |
| | CP | 15.05 ± 0.03c | 64.44 ± 0.18c | 14.26 ± 0.12a | 68.64 ± 0.54a | 0.79 ± 0.10d | 22.22 ± 2.95d |
| | PF | 14.84 ± 0.18c | 64.78 ± 0.62c | 12.88 ± 0.39b | 65.45 ± 0.80b | 1.96 ± 0.27c | 48.00 ± 2.00b |
| | CF | 20.96 ± 0.04b | 70.13 ± 0.05b | 12.15 ± 0.37c | 69.43 ± 0.36a | 8.81 ± 0.39b | 63.97 ± 0.32a |
| | SF | 32.34 ± 0.08a | 72.85 ± 0.03a | 9.95 ± 0.25d | 70.66 ± 0.85a | 22.40 ± 0.25a | 70.71 ± 0.36a |

*SOC* soil organic carbon, *POC* particulate organic carbon, *MOC* mineral organic carbon

increasing soil depth, and the contributions in aggregate varied between 38.54% to 80.80% and 22.22% to 74.81%, respectively. The organic carbon and carbon fraction content and their contributions in the 3–5 mm aggregates decrease with increasing soil profile, but still account for the majority of the karst soils.

### 3.4 Visualization and analysis of the spatial morphological distribution of soil pores in CT scanned aggregates.

In the multidimensional visualization of representative karst aggregates, pore space and soil are shown in white and black, respectively, in the binary image, and the spatial distribution of pore space is shown in yellow in the 3D image. As shown in Fig. 3, the soil pores were mainly distributed in the central areas of the aggregates. With increasing soil depth, the number of large pores in the multidimensional space of the aggregates all decreased significantly and the content of small pores increased. There are also large differences between the pore structures of the aggregates due to different land management practices. In the topsoil layer, the PF, CF and SF aggregates had relatively continuous tubular biological pores or root pores, with a network structure. Among them, the SF and CF aggregates were dominated by large complex porous pores with good uniform connectivity, while the PF pores were more sparsely distributed and less well connected. The CL and CP pores were mostly flat and elongated with a mixed distribution of fine, uneven pores and simple, isolated structures. With increasing soil depth, the soil pore structure became simpler and more isolated. Within the 20–40 cm soil layer of SF and CF, pore connectivity was also higher, with the distributions showing complex continuous network structures, with more cross pores.

The pore connectivity was next highest in PF. In contrast, the CL and CP pore shapes were mainly distributed in fine aggregates with less connectivity, and the number of small pores in CL was significantly higher than that in CP.

### 3.5 Quantification of the pore structure characteristics of aggregates

#### 3.5.1 Basic characteristics of pores

The pore structure of aggregates was quantified by digital image processing technology, as shown in Table 5. The porosity of all aggregates was within 20%, with the SF and CF aggregates having significantly higher porosity than the PF, CP and CL aggregates ($P < 0.05$). Furthermore, the porosity decreased with increasing soil depth. The increase in specific surface area indicated an improvement in the aggregate structure, and its distribution range was 0.631 ~ 0.960 μm. The specific surface areas of SF, CF and PF were significantly higher than those of CP and CL in the topsoil layer, while those of SF and CF were significantly higher than the other aggregates in the subsurface layer ($P < 0.05$). The soil structure showed a gradual improvement trend from the CL to SF. The pore throat is the narrowest part of the pore structure and determines the rate of material transport. In the topsoil layer, the pore throat numbers of the CL, CP and PF aggregates were significantly higher than those of the SF and CF aggregates ($P < 0.05$). The number of pore throats increased in the lower soil layer and was significantly higher in the CL aggregates than in the other aggregates, with no significant difference between CP and PF, but both had significantly higher values than SF and CF ($P < 0.05$). The number of aggregate pores in the upper soil layer followed the order SF > CF > PF > CL > CP, with significant differences among each aggregate ($P < 0.05$). The subsoil layer showed the order SF > CF > PF > CP > CL.

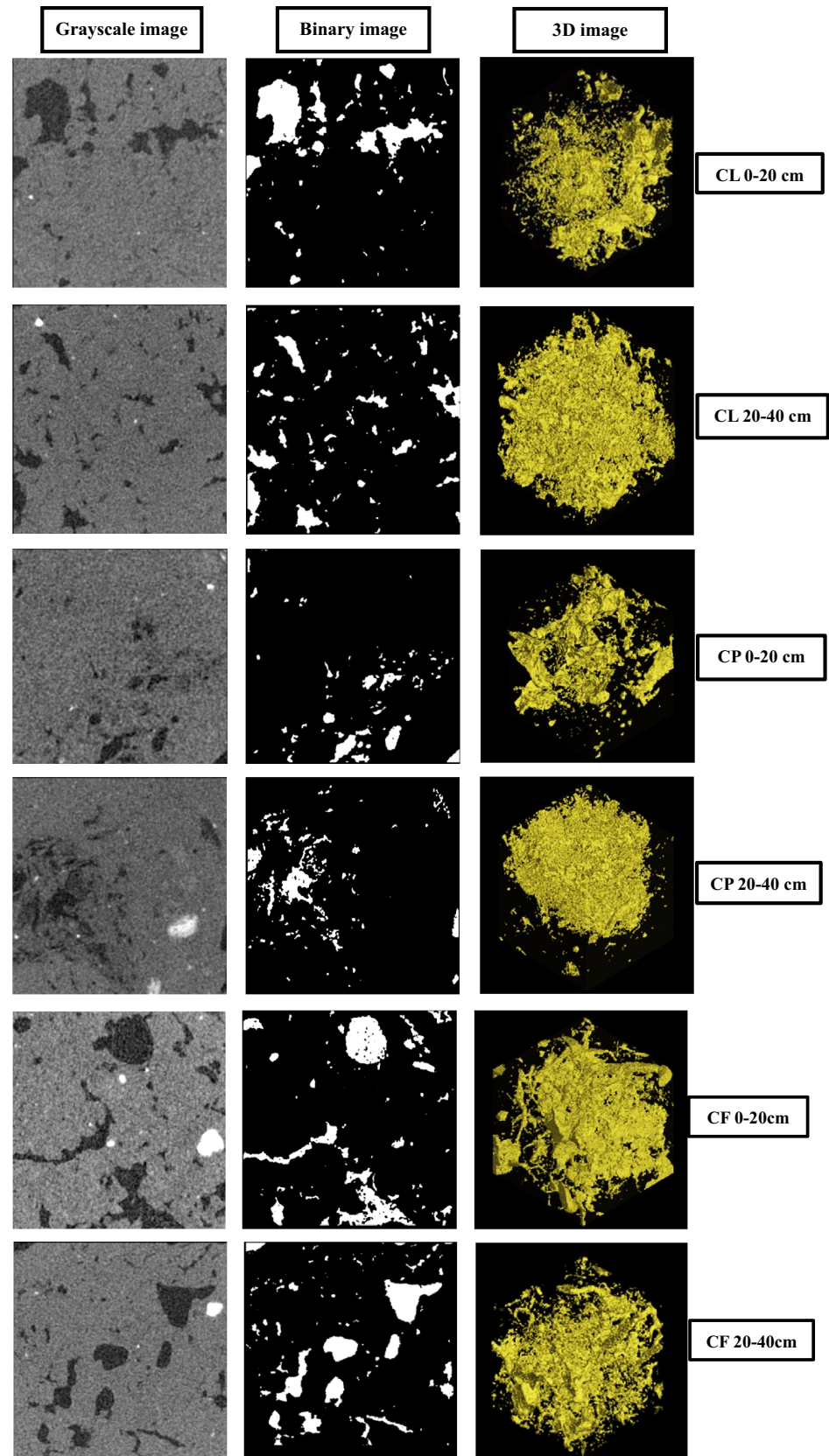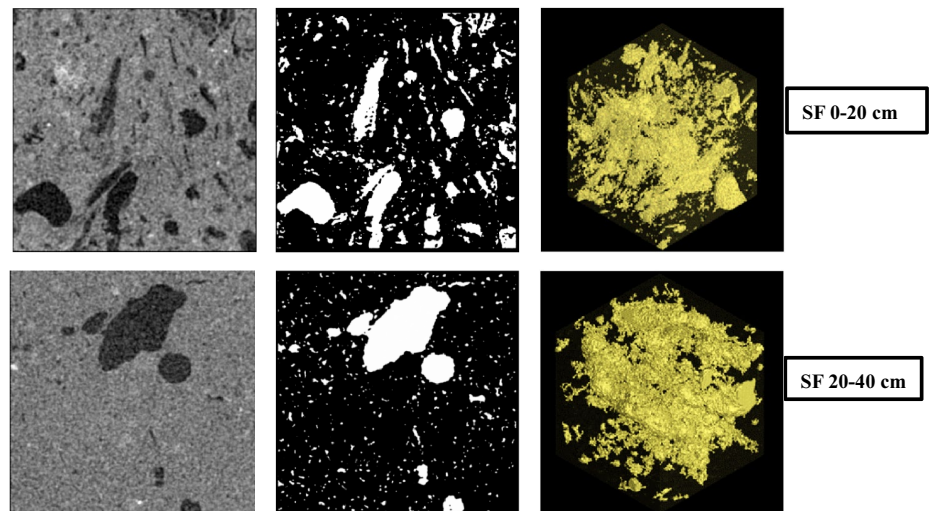**Fig. 3** Multidimensional image visualization structure of different land-use aggregate

**Fig. 3** (continued)



*CL* cultivated land, *CP* citrus plantation, *PF* plantation forest, *CF* coppice forest, *SF* secondary forest

The number of paths refers to the number of independent paths connecting two points within a pore structure. The numbers of paths in SF in the two soil layers were 54,561 and 50,185 pcs, respectively, which were significantly higher than those of the other aggregates, with a gradual decrease in the number of paths from SF to CL and a gradual deterioration in pore structure ($P < 0.05$). The pore tortuosity quantifies the degree of pore complexity. In this study, tortuosity varied from 1.47 to 12.31 and decreased with increasing soil depth. The CF and SF pore tortuosities were significantly higher than those of PF, CP and CL in the upper soil layers ($P < 0.05$). The pore tortuosity was highest in the subsoil of SF, followed by CF, CP and PF, with no significant difference, while the tortuosity in CL was the lowest ($P < 0.05$). More irregular pores were present in the topsoil aggregates, while there was a gradual increase in pore connectivity from CL to SF.
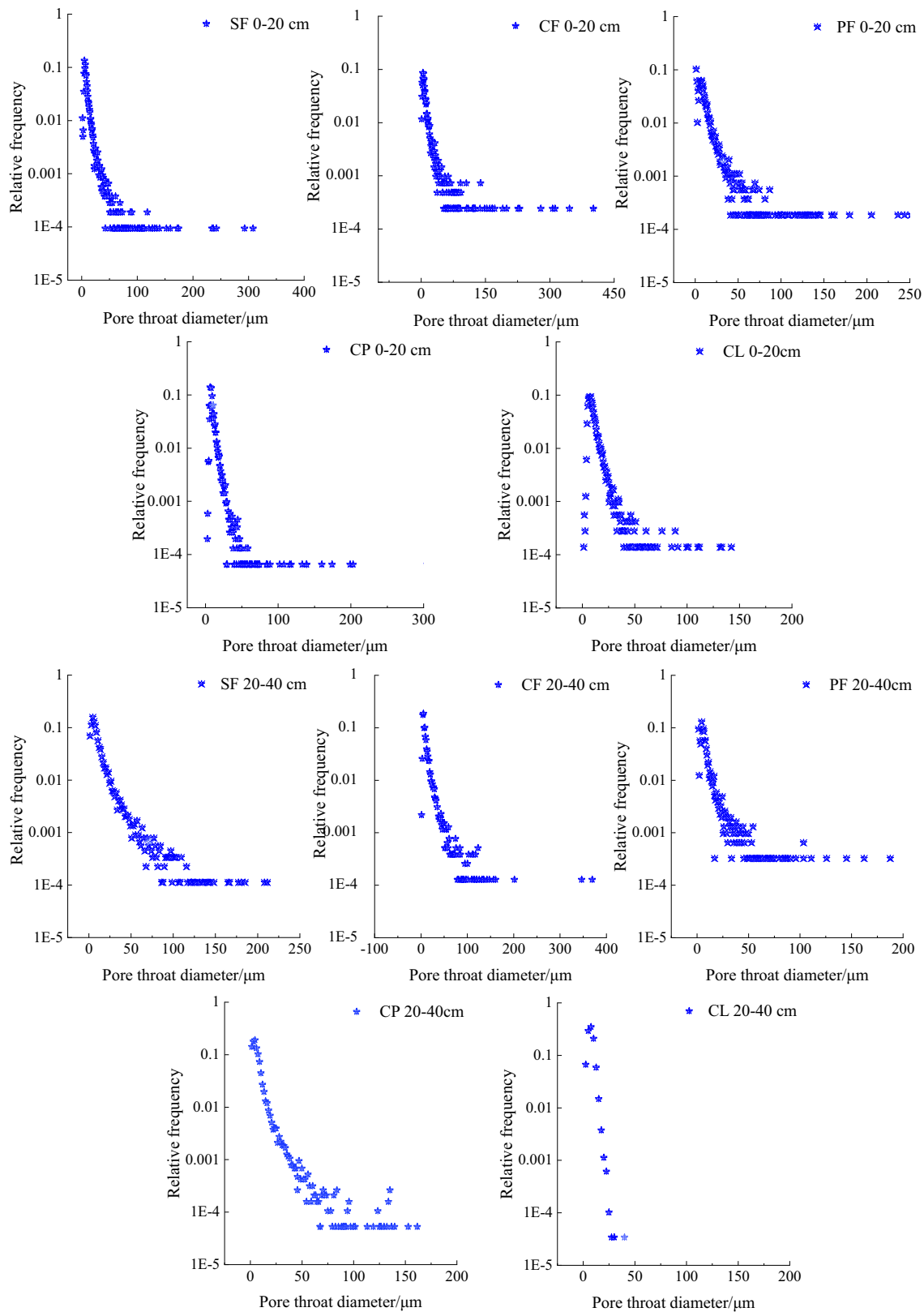
### 3.5.2 Diameter of the pore throat

To analyze the connectivity of the pore structure, the pore throat diameter of each aggregate was observed. In the 0–20 cm soil layer, the pore throat diameter distribution ranged from 1.32 μm to 401.76 μm (Fig. 4), with the maximum pore throat diameters being found in CF (401.76 μm), SF (308.31 μm), PF (243.92 μm), CP (203.00 μm) and CL (143.13 μm) in that order. The relative frequency of the pore throats increased and then decreased with increasing diameter, which was mainly concentrated within 0–20 μm, with the relative frequency following the order of CP (96.01%), CL (94.81%), PF (94.24%), SF (89.73%) and CF (87.55%). The CF and SF pore throats were larger in diameter and had better pore connectivity, while the PF, CP and CL pore throats were smaller in diameter and had poorer pore structure.

**Table 5** Basic pore characteristics parameters of aggregate

| Soil layer | Land type | PY/(%) | SSA/(um) | NPT/(pcs) | NPO/(pcs) | NPA/(pcs) | APL/(um) | PT |
|---|---|---|---|---|---|---|---|---|
| 0–20 cm | CL | 6.43cA | 0.743bA | 29227aA | 6999cA | 6089dA | 21.18bB | 4.82cA |
| | CP | 10.44bA | 0.710bA | 18947bA | 5185cA | 10512cA | 19.07bA | 6.39bcA |
| | PF | 12.31bA | 0.916aA | 11819cA | 9744cA | 11820cA | 28.07aA | 8.86bA |
| | CF | 14.32aA | 0.926aA | 8125dA | 16930bA | 21615bA | 30.23aA | 10.33aA |
| | SF | 16.53aA | 0.960aA | 5396dA | 42597aA | 54561aA | 31.67aA | 12.31aA |
| 20–40 cm | CL | 3.39cB | 0.600cB | 15279aB | 3030 dB | 3233cB | 15.92cB | 1.47cB |
| | CP | 4.25cB | 0.631cB | 8942bB | 4167 dB | 5401cB | 25.53bB | 3.94bB |
| | PF | 5.18cB | 0.720bA | 7191bB | 6455cB | 8157bB | 26.498bA | 4.46bB |
| | CF | 7.85bB | 0.864aA | 3096cB | 8251bA | 9273bA | 29.53aA | 5.09bA |
| | SF | 11.19aB | 0.880aB | 4272cB | 36409aB | 50185aA | 32.24aA | 7.48aB |

Capital letters in the same column refer to aggregates with significant difference in pore parameters between soil layers, and small letters refer to aggregates with significant difference between soil layers ($P < 0.05$)

*PY* porosity, *SSA* specific surface area, *NPT* number of pore throats, *NPO* number of pores, *NPA* number of paths, *APL* average path length, *PT* pore tortuosity

*CL* cultivated land, *CP* citrus plantation, *PF* plantation forest, *CF* coppice forest, *SF* secondary forest

**Fig. 4** Distribution of pore throat diameters and relative frequencies of aggregate

In the 20–40 cm soil layer (Fig. 4), the pore throat diameters were also dominantly 0–20 μm, and the relative frequencies were all greater than those in the upper surface layer, in the order of CL (99.91%), CP (95.41%), PF (93.34%), CF (89.81%) and SF (87.99%). The pore throat diameter decreased with increasing soil depth, while the pore throat diameter increased gradually from CL to SF.

### 3.5.3 Equivalent diameter

Pores are classified into 3 classes according to their equivalent diameter, macropores (> 100 μm), capillary pores (30–100 μm) and storage pores (< 30 μm) (Warner et al. 1989; Luxmoore et al. 1990). In this study, the equivalent diameters range from 1.355 μm to 806.690 μm, including the three types of pores mentioned above.

As shown in Fig. 5, the pores of karst aggregate were mainly storage pores < 30 μm, accounting for 50.21% ~ 79.02%. The average values of storage pore space for each aggregate in the 0–20 cm soil layer yielded the order of SF (28.69 μm), CF (26.16 μm), PF (20.99 μm), CP (16.24 μm) and CL (15.71 μm). Among them, the storage pore contents of CL, CP and PF were much greater than those of SF and CF. The percentage of capillary pores ranged from 15.06% to 37.25%, making them less common than storage pores, and the pattern of variation in the mean value was SF (66.35 μm) > PF (56.58 μm) > CF

(54.16 μm) > CL (45.95 μm) > CP (43.39 μm). Macropores exhibited the lowest content, ranging from 3.42% to 13.95%, and the mean values yielded the order of CF (227.20 μm) > SF (196.77 μm) > PF (195.79 μm) > CP (158.18 μm) > CL (146.55 μm).

The pore equivalent diameter of the subsoil layer followed a similar trend to that of the topsoil layer, with both the mean and percentage decreasing with increasing soil depth. Among the aggregates, the SF, CF and PF storage pore contents increased significantly, while the CL and CP storage pore contents increased to a lesser extent. From CL to SF, the storage pore content gradually decreased, but it still predominated, while the macropore and capillary pore contents gradually increased, and the soil structure improved. The depth of the soil layer is an important factor affecting the pore characteristics of the soil.

## 3.6 Identification of the pore structure and stability of aggregates and influencing factors

To dissect the relationship between aggregate cementing material, pore structure and stability, a correlation analysis was carried out, as shown in Fig. 6. There was a highly significant positive correlation between SOC and POC in the carbon fraction and MWD$_{FW}$ and MWDws values ($P < 0.01$). The MOC of the carbon components had no significant correlation with the stability parameters. In addition, SOC was
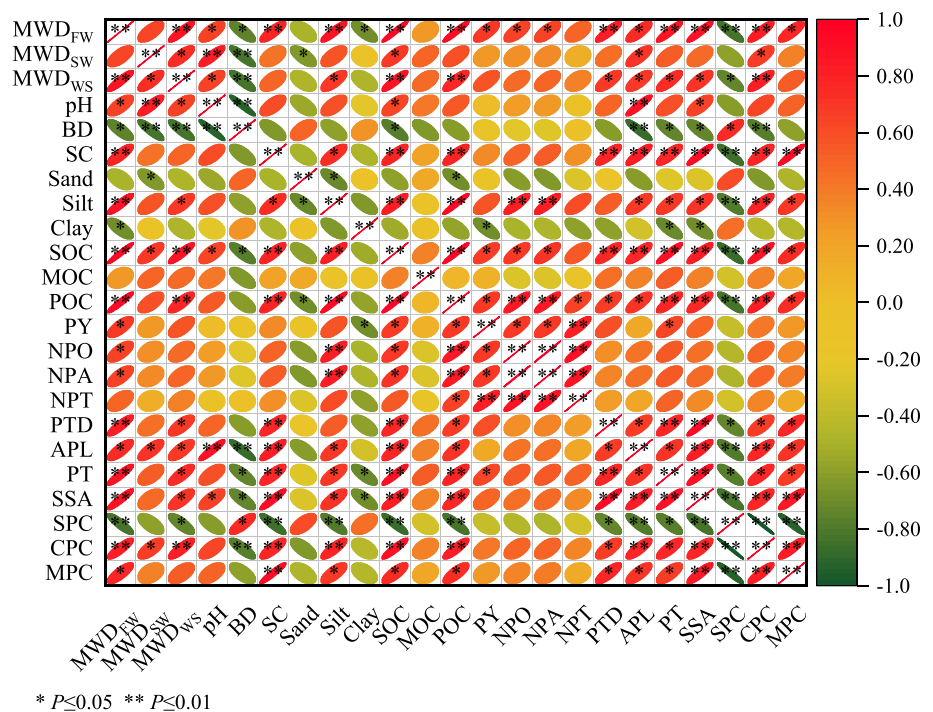
**Fig. 5** Characteristics of the pore equivalent distribution of aggregate
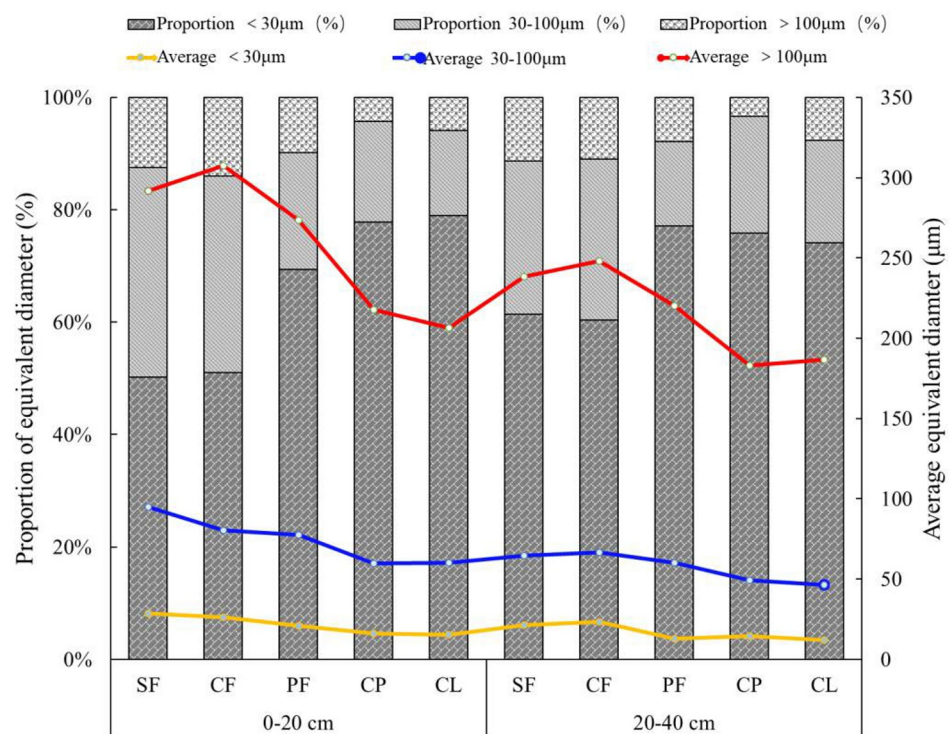


*CL* cultivated land; *CP* citrus plantation, *PF* plantation forest, *CF* coppice forest, *SF* secondary forest

**Fig. 6** Correlation analysis



* $P \leq 0.05$  ** $P \leq 0.01$

*SPC* storage pore content*, CPC* capillary pore content*, MPC* macropore content, * indicates significant correlation ($P < 0.05$), ** indicates highly significant correlation ($P < 0.01$)

significantly and negatively correlated with soil bulk density, while SOC and POC were significantly positively correlated with many parameters characterizing pore structure connectivity (such as porosity, pore number and pore throat diameter) and soil water content ($P < 0.05$). Therefore, an increase in soil SOC and POC content will increase soil pore connectivity, enhance soil solute transport and improve soil structure. We further hypothesized that SOC may indirectly affect the stability of aggregates by affecting the morphological characteristics of soil pores. We found that clay content was significantly and negatively correlated with porosity, tortuosity, specific surface area and MWD$_{FW}$, while silt was significantly or highly significantly and positively correlated with MWD$_{FW}$, MWDws and several pore parameters (number of pores, number of paths, average path length, etc.) and negatively correlated with storage pores ($P < 0.05$). Soil texture also has some influence on the pore structure and stability of aggregates.

We fully fitted the data to build an SEM based on correlation analysis. The causes and main pathways to the differences in aggregate structure caused by cementing substances were explained: cementing substances work on the soil pore structure and indirectly cause differences in aggregate stability.

The structural pathways are shown in Fig. 7A. SOC has a positive relationship with porosity, pore throat diameter

and silt (path coefficients of 0.897, 0.770 and 0.717), indirectly affecting the stability parameter MWD and negatively affecting storage pore space (-0.872). It is worth noting that the pore throat diameter positively affected the specific surface area (0.911), soil water content (0.913) and ultimately, the MWD by influencing the aggregate porosity (0.594). SEM analysis verifies our hypothesis that SOC was able to improve aggregate stability by directly or indirectly increasing porosity and inhibiting storage pore generation.

The POC then directly determined the number of capillary pores (0.832) and indirectly influenced the pore throat diameter (0.665) to increase the porosity (0.592) and ultimately the aggregate stability MWD (Fig. 7A, B). Alternatively, it directly determined the number of paths (0.969) and indirectly caused an increase in porosity (0.690) and ultimately the MWD. In addition, the positive effect of the silt contents on the MWD was observed, but its effect was not significant (0.370 and 0.408) (Fig. 7A, B). Therefore, the SOC and POC contents of limestone soils were important factors influencing the stability of aggregates, while increasing soil porosity and suppressing the number of storage pores were the main mechanisms. While the mechanical composition of the soil was correlated with the content of cementitious materials and aggregate stability, it did not constitute the dominant factor affecting aggregate stability.
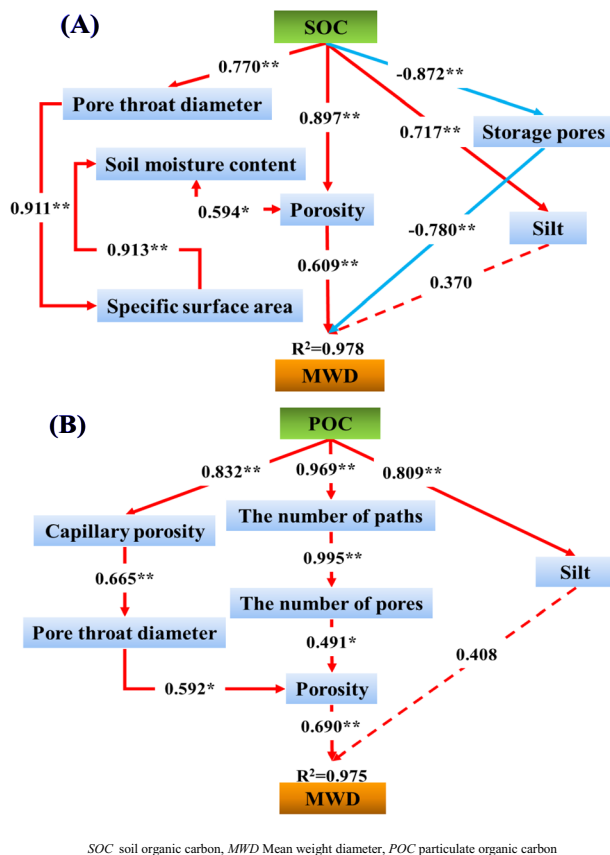
**(A)**

**(B)**

*SOC* soil organic carbon, *MWD* Mean weight diameter, *POC* particulate organic carbon

**Fig. 7** Structural equation model

## 4 Discussion

### 4.1 Stability characteristics and main fragmentation mechanisms of karst aggregates

As the basic unit of soil structure (Mikha and Rice 2004), the observation of stability characteristics, the investigation of fragmentation mechanisms and the analysis of the main influencing factors are important references in the evaluation of soil quality (Bronick and Lal 2005). The main fragmentation mechanisms of the karst aggregates were slaking and mechanical destruction. The stability of aggregates showed the following trend: SF > CF > PF > CP > CL (Table 3). Due to the rapid saturation of aggregates with water under the FW treatment, cementation between soil particles gradually weakens, while the air inside the aggregate rapidly compresses and bursts, causing the aggregate to break. Mechanical damage from external forces simulated by the WS treatment was also an important factor in the stability of aggregates. As agricultural land, the CL and CP experience repeated human tilling of the soil during production, which causes extrusion and deformation of the soil skeleton structure under external forces, affecting the cementation between soil particles and

causing structural damage and loss of stability of the soil. In contrast, the soils in PF were relatively less frequently disturbed, and the aggregates were more stable. There were few little external influences on the SF and CF soils, and the soil particles formed stable aggregates via the cohesive action of transient polysaccharides and fungal hyphae associated with microorganisms and plant roots (Tisdall and Oades 1982). Previous studies showed a correlation between soil fragmentation and pore structure (Hallett et al. 1995), but in the case of aggregate pore structure, numerous factors influenced the variations in the pore distribution characteristics.

### 4.2 Variation in the pore structure characteristics of karst aggregate and the main causes

The depth of the soil layer was an important factor influencing the pore structure of aggregates (Yu et al. 2019). In this study, the parameters characterizing pore connectivity (number of pores, porosity, tortuosity, etc.) all decreased with increasing soil depth (Table 5). In the CT scan images, the pore network structure of the karst aggregates tended to change from large, cross-complexed pores to smaller, simpler pores as the depth of the soil layer increased (Fig. 3), which was consistent with the findings of Qiao et al. (2021). This may be related to the distribution of plant roots. The mechanical penetration and extrusion of vegetation roots increase the number of surface soil pores, while roots contribute to the carbon sequestration of the soil, and the mutually beneficial relationship between the two promoted the further development of surface soil pores (Ferro et al. 2013). The variability in the pore structure of aggregates between representative sample sites in karst areas was likely related to differences in the SOC content of the main soil cementing material.

Cementitious material is an important parameter affecting the pore characteristics of soils (Zhou et al 2012; Guo et al 2020; Mustafa et al 2020). Related studies have shown a correlation between SOC and soil porosity (Lu et al. 2014; Zhao et al. 2020), which is consistent with the results of this study (Fig. 6). SOC can act on soil mineral particles to aggregate them into microaggregates, which then form larger aggregates, promoting the development of aggregate pore structures and the transformation of existing pores to larger pore structures (Fang et al. 2018). Meanwhile, porous structures can enhance soil microbial functions and activities, further contributing to increased pore development and pore abundance (Kravchenko and Guber 2016). Our study also showed a significant positive correlation between the SOC content and the porosity, number of pores and number of pathways (Fig. 6). Thus, the SF and CF aggregates, which had higher SOC contents, had greater porosities and greater numbers of pores, whereas the PF, CL and CP aggregates had lower SOC

contents, lower porosities and lower numbers of pores (Table 5). This is also related to the characteristics of soils in karst areas. Although the nutrient content of limestone soils is relatively high compared to red soils at the same latitude, they are sensitive to anthropogenic disturbances, and reclamation can lead to a drastic reduction in nutrient content, including colloidal material (Barral et al. 1998), causing damage to the soil structure. Thus, the 3D structure of the pores similarly showed that the less disturbed SF and CF aggregates had a large number of internal pores with tubular connected macropores, while the CL and CP aggregates had fine pores and simple isolated structures (Fig. 3).

To quantify the extent and mechanism of the influence of the SOC in aggregates in karst areas on soil microstructure, SOC was further differentiated into POC and MOC (John et al. 2005; Gregorich et al. 2006). The results of the correlation analysis showed that the POC rather than the MOC in the carbon fraction was the dominant factor influencing the differences in the structural properties of the soil (Fig. 6). This is related to the structure and nature of the carbon component. As the transitional form of organic carbon between fresh plant and animal residues and humified organic matter, POC has a very rapid turnover rate (Besnard et al. 1996). Its chemical structure contains a large number of hydroxyl and alkyl groups, which bind soil particles and encourage aggregation around the POC to form stable aggregate structures (Tisdal and Oades 1982; Golchin et al. 1994), a process that is accompanied by the creation of a large number of pore structures. When the number of soil pores and connectivity increases, the rate of decomposition of SOC into POC accelerates due to frequent air exchange within the soil (Kravchenko et al. 2015), resulting in an increased soil POC content, a process that triggers significant $CO_2$ emissions and again promotes soil pore production (Gryze, et al. 2006; Feeney, et al. 2006; Crawford et al. 2012; Helliwell, et al. 2014). Therefore, POC in the carbon fraction is an important variable influencing the formation of the soil microstructure. MOC, also known as inert organic carbon, varies over cycles of tens to thousands of years (Dalal and Chan 2001), with a high resistance to both physical and chemical decomposition (Wairiu and Lal 2003). Therefore, the effect of MOC changes on variations in soil pore structure is not significant.

Clay is also considered to be one of the consolidating substances that affects the pore structure of soils, with an increase in the clay content significantly affecting the cementing capacity of soils and improving the structural stability of aggregates (Ma et al. 2015). In this study, karst aggregate pores were dominated by < 30 μm storage pores (Fig. 5), which may be related to the texture of the soils in the study area. Previous studies have shown that a higher clay and silt sized particle content reduces soil porosity, while sandy soils tend to have higher porosity (Park and

Smucker 2005; Zhao et al. 2020). The mechanical composition of the karst soils in this study was dominated by clay and silt grains with a clay-heavy texture (Table 2), which may be the main cause of the predominance of storage pores in all of the soil pores. However, the soil structure may be influenced to various extents by the type and content of cementing material in the aggregates, as well as other factors (Jozefaciuk et al. 2015). Thus, according to the SEM constructed in this study, the soil mechanical composition played a less important role in influencing the microstructure of aggregates compared with other cementing substances (Fig. 7).

## 4.3 Relationship among the SOC, carbon fractions and pore characteristics of karst aggregates and aggregate stability

In this study, an SEM was used to further analyze the relationship among the main cementing substances, soil micropore characteristics and aggregate stability (Fig. 7A, B). The results showed that the SOC and POC, the main cementing substances of karst aggregates, were indirect determinants of the structural stability parameter MWD, while increasing soil porosity and decreasing storage pore space, either directly or indirectly, were the main pathways. This may be related to the conditions of the study area and the intensity of anthropogenic disturbances. Limited by natural conditions, karst soils are extremely susceptible to nutrient deficiencies caused by the leaching of N and P (Fenton et al. 2017; Xiao et al. 2019), which restricts crop growth. In severely degraded ecosystems agricultural land requires high levels of inorganic fertilizer inputs to meet production needs. Previous studies have found that the effects of fertilization can affect the content and distribution of aggregated colloidal materials (Bronick and Lal 2005) and even promote the decomposition of soil colloids, thereby deteriorating the soil structure and reducing the soil porosity (Haynes and Naidu 1998; Zhou et al. 2016). In addition, tillage can also lead to the accelerated decomposition and loss of cementing substances, especially POC (Franzluebbers and Arsha 1997), causing an imbalance in the carbon fraction and destroying the original skeletal structure of the soil pore space. The change in the cementing material's ability to consolidate soil particles in turn affects the morphological characteristics and arrangement of soil pores (Schweizer et al. 2019). Therefore, the difference in pore structure among aggregates in the study area results from differences in the soil SOC content and composition. As an abiotic factor affecting the rate of soil carbon mineralization, the soil pore structure can also control the fate and transformation of organic carbon in colloidal material, and its compartment effect is the physical basis for the sequestration of cementitious material (Smucker et al. 2010). This stems primarily from the fact that pore structure

can influence microbial activity by determining the accessibility of organic substrates by microorganisms or hydrolytic enzymes through physical barriers (Killham et al. 1993), or by regulating the availability of water and oxygen within the aggregate (Sexstone et al. 1985), thereby altering the rate of organic carbon decomposition. In addition, the process of soil carbon sequestration also generates a positive feedback effect on soil structure and increases soil connectivity. Therefore, there was also a significant positive correlation among soil SOC, POC and aggregate porosity and other parameters characterizing pore connectivity (Fig. 6).

In addition, the mechanical damage (tilling) simulated by the WS treatment is one of the main mechanisms of structural slaking of karst aggregates (Table 3). External forces applied during frequent tillage could reduce the number of pores and decrease the porosity of larger pores and inversely increase the number of smaller pores (Wang et al. 2019), which isolates the pore structure and hinders soil water and solute transport. Therefore, CL and CP aggregates with frequent disturbances have poor pore connectivity, a large number of small pores and poor stability. Most of the karst CF and SF sample sites were the products of natural restoration after arable land was returned to forest and grass or the native vegetation was completely destroyed. A large amount of litter was returned to the soil during the long-term self-healing process, which increased the soil SOC content and contributed to the soil aggregation process in multiple ways as an important soil cementing substance, effectively improving the stability of aggregates effectively. At the same time, with the increase in the rooting of underground vegetation, plant roots penetrated and extended into the soil, causing an increase in soil pore permeability and a decrease in bulk density, which improved the soil structure (Gill et al. 2010; Zhou et al. 2012). These changes to the soil microenvironment allowed for access to sufficient gas and water for microorganisms to thrive, laterally increasing microbial activity and the rate of decomposition of plant residues (Strong et al. 2004). Thus, the greater pore connectivity of the SF and CF aggregates directly enhanced their aggregate stability to some extent.

A combination of organic and inorganic fertilizer application has been demonstrated to produce a loose and porous soil structure (Zhou et al. 2013). The application of organic fertilizers is effective for increasing the number of macropores and for increasing pore connectivity (Ferro et al. 2012a, b), while the use of low tillage and no-tillage methods and the application of organic fertilizers are also considered effective for increasing the soil POC content (Fortuna et al. 2003; Álvaro-Fuentes et al. 2008). Therefore, the rational planning of CL and CP fertilization and tillage practices in karst areas could be an effective way to meet the dual needs for achieving high agricultural

production and improved soil pore structure. Increasing the content of soil cementitious materials and reducing disturbance frequencies could be decisive factors affecting the stability of aggregates. Furthermore, CT scanning is an effective means to reveal the degree of development and influencing factors for aggregate formation.

# 5 Conclusion

CT scanning was used to analyze the structural characteristics of the pore spaces of karst aggregates in this study. The LB method was used to explore the stability and main fragmentation mechanisms of the aggregates. The stability and pore structure characteristics of aggregates in five land-use types in karst areas and their coupled relationships with organic carbon and its components were analyzed with an SEM. The significant differences were found in the stability of the aggregates between land-use types in the study area, as follows: SF > CF > PF > CP > CL. These were related to the differences in frequency of anthropogenic disturbances and the content of cementitious materials. Slaking and mechanical damage from tillage were the main mechanisms of karst soil aggregate destruction. The pore distribution of the aggregates was dominated by storage pores < 30 μm in size, with pore throat diameters concentrated in the range of 0–20 μm, which was related to the clayey texture of the soils in the study area. SF and CF, followed by PF, had the best pore connectivity among the land-use types. In contrast, the CP and CL aggregates, which were heavily fertilized with inorganic fertilizers and were frequently disturbed, had predominantly uneven pore distributions and poor connectivity. Correlation analysis showed that the POC component of the carbon fraction was the dominant factor influencing the pore characteristics and structural stability of the soils. SEM analysis revealed that the cementing substances SOC and POC could alter aggregate stability by directly or indirectly influencing the soil porosity and storage pore space. In order to meet the two-way needs of production and improving soil structure, it is an effective way to mix fertilizer reasonably and reduce disturbance frequency for agricultural production land.

## Declarations

**Conflict of interest** No conflict of interest exists in the submission of this manuscript, and manuscript is approved by all authors for publication. I would like to declare on behalf of my co-authors that the work described is our original research that has not been published previously, nor under consideration for publication elsewhere, in whole

or in part. All the authors listed have approved the submission of the manuscript enclosed.

# References

Álvaro-Fuentes J, López MV, Cantero-Martinez C, Arrúe JL (2008) Tillage effects on soil organic carbon fractions in Mediterranean dryland agroecosystems. Soil Sci Soc Am J 72(2):541–547. https://doi.org/10.2136/sssaj2007.0164

Ananyeva K, Wang W, Smucker, AJM, Rivers ML, Kravchenko AN (2013) Can intra-aggregate pore structures affect the aggregate's effectiveness in protecting carbon? Soil Biol Biochem 57:868–875. https://doi.org/10.1016/j.soilbio.2012.10.019

Bronick CJ, Lal R (2005) Soil structure and management: a review. Geoderma 124(1–2):3–22. https://doi.org/10.1016/j.geoderma.2004.03.005

Besnard E, Chenu C, Balesdent J, Puget P, Arrouays D (1996) Fate of particulate organic matter in soil aggregates during cultivation. Eur J Soil Sci 47(4):495–503. https://doi.org/10.1111/j.1365-2389.1996.tb01849.x

Barral MT, Arias M, Guérif J (1998) Effects of iron and organic matter on the porosity and structural stability of soil aggregates. Soil Till Res 46(3–4):261–272. https://doi.org/10.1016/s0167-1987(98)00092-0

Crawford JW, Deacon L, Grinev D, Harris JA, Ritz K, Singh BK, Young I (2012) Microbial diversity affects self-organization of the soil-microbe system with consequences for function. J R Soc Interface 9(71):1302–1310. https://doi.org/10.1098/rsif.2011.0679

Cercioglu M, Anderson SH, Udawatta RP, Haruna SI (2018) Effects of cover crop and biofuel crop management on computed tomography-measured pore parameters. Geoderma 319:80–88. https://doi.org/10.1016/j.geoderma.2018.01.005

Costa PAD, Mota JCA, Romero RE, Freire AG, Ferreira TO (2014) Changes in soil pore network in response to twenty-three years of irrigation in a tropical semiarid pasture from northeast Brazil. Soil till Res 137:23–32. https://doi.org/10.1016/j.still.2013.11.004

Cássaro FAM, Durand ANP, Gimenez D, Vaz CMP (2017) Pore-size distributions of soils derived using a geometrical approach and multiple resolution microCT images. Soil Sci Soc Am J 81(3):468–476. https://doi.org/10.2136/sssaj2016.09.0291

Deurer M, Grinev D, Young I, Clothier BE, Müller K (2009) The impact of soil carbon management on soil macropore structure: a comparison of two apple orchard systems in New Zealand. Eur J Soil Sci 60(6):945–955. https://doi.org/10.1111/j.1365-2389.2009.01164.x

Dalal RC, Chan KY (2001) Soil organic matter in rainfed cropping systems of the Australian cereal belt. Aust J Soil Res 39(3):435–464. https://doi.org/10.1071/SR99042

Dal Ferro N, Berti A, Francioso O, Ferrari E, Matthews GP, Morari F (2012a) Investigating the effects of wettability and pore size distribution on aggregate stability: the role of soil organic matter and the humic fraction. Eur J Soil Sci 63(2):152–164. https://doi.org/10.1111/j.1365-2389.2012.01427.x

Edwards AP, Bremner JM (1967) Microaggregates in soils. Eur J Soil Sci 18(1):64–73. https://doi.org/10.1111/j.1365-2389.1967.tb01488.x

Ferro ND, Delmas P, Duwig C, Simonetti G, Morari F (2012b) Coupling X-ray microtomography and mercury intrusion porosimetry to quantify aggregate structures of a cambisol under different fertilisation treatments. Soil till Res 119:13–21. https://doi.org/10.1016/j.still.2011.12.001

Ferro ND, Charrier P, Morari F (2013) Dual-scale micro-CT assessment of soil structure in a long-term fertilization experiment. Geoderma 204–205:84–93. https://doi.org/10.1016/j.geoderma.2013.04.012

Fang H, Ling Y, Zhou H (2018) Effects of straw incorporation on paddy soil structure in rice-wheat rotation system. Trans Chinese Soc Agric Machinery 49:297–302. https://doi.org/10.6041/j.issn.1000-1298.2018.04.034

Feng Y, Wang JM, Liu T, Bai ZK, Reading L (2019) Using computed tomography images to characterize the effects of soil compaction resulting from large machinery on three-dimensional pore characteristics in an opencast coal mine dump. J Soils Sediments 19(3):1467–1478. https://doi.org/10.1007/s11368-018-2130-0

Feng Y, Wang M, Bai ZK, Reading L, Jing ZR (2020) Three-dimensional quantification of macropore networks of different compacted soils from opencast coal mine area using X-ray computed tomography. Soil till Res 198:104567. https://doi.org/10.1016/j.still.2019.104567

Feeney DS, Crawford JW, Daniell T, Hallett PD, Nunan N, Ritz K, Rivers M, Young IM (2006) Three-dimensional microorganization of the soil–root–microbe system. Microb Ecol 52(1):151–158. https://doi.org/10.1007/s00248-006-9062-8

Fenton O, Mellander PE, Daly K, Wall DP, Jahangir MMR, Jordan P, Hennessey D, Huebsch M, Blum P, Vero S, Richards KG (2017) Integrated assessment of agricultural nutrient pressures and legacies in karst landscapes. Agric Ecosyst Environ 239:246–256. https://doi.org/10.1016/j.agee.2017.01.014

Franzluebbers AJ, Arshad MA (1997) Particulate organic carbon content and potential mineralization as affected by tillage and texture. Soil Sci Soc Am J 61(5):1382–1386. https://doi.org/10.2136/sssaj1997.03615995006100050014x

Fortuna A, Harwood RR, Paul EA (2003) The effects of compost and crop rotations on carbon turnover and the particulate organic matter fraction. Soil Sci 168(6):434–444. https://doi.org/10.1097/01.ss.0000075288.53382.91

Gryze SD, Jassogne L, Six J, Bossuyt H, Wevers M, Merckx R (2006) Pore structure changes during decomposition of fresh residue: X-ray tomography analyses. Geoderma 134(1–2):82–96. https://doi.org/10.1016/j.geoderma.2005.09.002

Guo YF, Fan RQ, Zhang XP, Zhang Y, Wu DH, McLaughlin N, Zhang SX, Chen XW, Jia SX, Liang AZ (2020) Tillage-induced effects on SOC through changes in aggregate stability and soil pore structure. Sci Total Environ 703:134617. https://doi.org/10.1016/j.scitotenv.2019.134617

Garbout A, Munkholm LJ, Hansen SB (2013a) Tillage effects on topsoil structural quality assessed using X-ray CT, soil cores and visual soil evaluation. Soil till Res 128:104–109. https://doi.org/10.1016/j.still.2012.11.003

Garbout A, Munkholm LJ, Hansen SB (2013b) Temporal dynamics for soil aggregates determined using X-ray CT scanning. Geoderma 204–205:15–22. https://doi.org/10.1016/j.geoderma.2013.04.004

Gargiulo L, Mele G, Terribile F (2013) Image analysis and soil micromorphology applied to study physical mechanisms of soil pore development: An experiment using iron oxides and calcium carbonate. Geoderma 197–198:151–160. https://doi.org/10.1016/j.geoderma.2013.01.008

Garten CT, Post WM, Hanson PJ, Cooper LW (1999) Forest soil carbon inventories and dynamics along an elevation gradient in the southern Appalachian Mountains. Biogeochemistry 45(2):115–145. https://doi.org/10.1023/a:1006121511680

Gregorich EG, Beare MH, McKim UF, Skjemstad JO (2006) Chemical and biological characteristics of physically uncomplexed organic matter. Soil Sci Soc Am J 70(3):975–985. https://doi.org/10.2136/sssaj2005.0116

Golchin A, Oades JM, Skjemstad JO, Clarke P (1994) Study of free and occluded particulate organic matter in soils by solid state 13C CP-MASNMR spectroscopy and scanning electron microscopy. Aust J Soil Res 32(2):285–309. https://doi.org/10.1071/SR9940285

Gill JS, Sale PWG, Peries RR, Tang C (2010) Corrigendum to "Changes in soil physical properties and crop root growth in dense sodic

subsoil following incorporation of organic amendments." Field Crop Res 116(1–2):205–2051. https://doi.org/10.1016/j.fcr.2009.11.011

Haynes RJ, Naidu R (1998) Influence of lime, fertilizer and manure applications on soil organic matter content and soil physical conditions: a review. Nutr Cycl Agroecosys 51(2):123–137. https://doi.org/10.1023/a:1009738307837

Helliwell JR, Miller AJ, Whalley WR, Mooney SJ, Sturrock CJ (2014) Quantifying the impact of microbes on soil structural development and behaviour in wet soils. Soil Biol and Biochem 74:138–147. https://doi.org/10.1016/j.soilbio.2014.03.009

Hallett PD, Dexter AR, Seville JPK (1995) The application of fracture mechanics to crack propagation in dry soil. Eur J Soil Sci 46(4):591–599. https://doi.org/10.1111/j.1365-2389.1995.tb01355.x

John B, Yamashita T, Ludwig B, Flessa H (2005) Storage of organic carbon in aggregate and density fractions of silty soils under different types of land use. Geoderma 128(1–2):63–79. https://doi.org/10.1016/j.geoderma.2004.12.013

Jozefaciuk G, Czachor H, Lamorski K, Hajnos M, Swieboda R, Franus W (2015) Effect of humic acids, sesquioxides and silica on the pore system of silt aggregates measured by water vapour desorption, mercury intrusion and microtomography. Eur J Soil Sci 66(6):992–1001. https://doi.org/10.1111/ejss.12299

Kan XQ, Cheng JH, Hou F (2020) Response of preferential soil flow to different infiltration rates and vegetation types in the karst region of southwest China. Water 12(6):1778. https://doi.org/10.3390/w12061778

Kravchenko AN, Negassa WC, Guber AK, Rivers ML (2015) Protection of soil carbon within macro-aggregates depends on intra-aggregate pore characteristics. Sci Rep 5:16261. https://doi.org/10.1038/srep16261

Kravchenko AN, Guber AK (2016) Soil pores and their contributions to soil carbon processes. Geoderma 287:31–39. https://doi.org/10.1016/j.geoderma.2016.06.027

Killham K, Amato M, Ladd JN (1993) Effect of substrate location in soil and soil pore water regime on carbon turnover. Soil Biol Biochem 25(1):57–62. https://doi.org/10.1016/0038-0717(93)90241-3

Liu CC, Liu YG, Guo K, Wang SJ, Liu HM, Zhao HW, Qiao XG, Hou DJ, Li SB (2016) Aboveground carbon stock, allocation and sequestration potential during vegetation recovery in the karst region of southwestern China: A case study at a watershed scale. Agric Ecosyst Environ 235:91–100. https://doi.org/10.1016/j.agee.2016.10.003

Le Bissonnais Y (1996) Aggregate stability and assessment of soil crustability and erodibility: I Theory and methodology. Eur J Soil Sci 47(4):425–437. https://doi.org/10.1111/j.1365-2389.1996.tb01843.x

Lu RK (2000) Analytical methods for soil and agro-chemistry (In Chinese) Beijing: China Agricultural Science and Technology Press

Luxmoore RJ, Jarding PM, Wilson GV, Jones JR, Zelazny LW (1990) Physical and chemical controls of preferred path flow through a forested hillslope. Geoderma 46(1–3):139–154. https://doi.org/10.1016/0016-7061(90)90012-x

Lu SG, Malik Z, Chen DP, Wu CF (2014) Porosity and pore size distribution of Ultisols and correlations to soil iron oxides. CATENA 123:79–87. https://doi.org/10.1016/j.catena.2014.07.010

Larsbo M, Koestel J, Kätterer T, Jarvis N (2016) Preferential transport in macropores is reduced by soil o carbon. Vadose Zone J 15(9):1–7. https://doi.org/10.2136/vzj2016.03.0021

Mikha MM, Rice CW (2004) Tillage and manure effects on soil and aggregate-associated carbon and nitrogen. Soil Sci Soc Am J 68(3):809–816. https://doi.org/10.2136/sssaj2004.8090

Ma RM, Jiang Y, Liu B, Fan HM (2020) Effects of pore structure characterized by synchrotron-based micro-computed tomography on aggregate stability of black soil under freeze-thaw cycles. Soil till Res 207:104855. https://doi.org/10.1016/j.still.2020.104855

Ma RM, Cai CF, Li ZX, Wang JG, Xiao TQ, Peng GY, Yang W (2015) Evaluation of soil aggregate microstructure and stability under wetting and drying cycles in two Ultisols using synchrotron-based X-ray micro-computed tomography. Soil till Res 149:1–11. https://doi.org/10.1016/j.still.2014.12.016

Menon M, Jia X, Lair GJ, Faraj PH, Blaud A (2015) Analysing the impact of compaction of soil aggregates using X-ray microtomography and water flow simulations. Soil Tillage Res 150:147–157. https://doi.org/10.1016/j.still.2015.02.004

Mustafa A, Xu MG, Shah SAA, Abrar MM, Sun N, Wang BR, Cai ZJ, Saeed Q, Naveed M, Mehmood K, Núñez-Delgado A (2020) Soil aggregation and soil aggregate stability regulate organic carbon and nitrogen storage in a red soil of southern China. J Environ Manage 270:110894. https://doi.org/10.1016/j.jenvman.2020.110894

Nunan N, Ritz K, Rivers M, Feeney DS, Young IM (2006) Investigating microbial micro-habitat structure using X-ray computed tomography. Geoderma 133(3–4):398–407. https://doi.org/10.1016/j.geoderma.2005.08.004

Ojeda G, Alcaiz JM, Bissonais YL (2008) Differences in aggregate stability due to various sewage sludge treatments on a Mediterranean calcareous soil. Agric Ecosyst Environ 125(1–4):48–56. https://doi.org/10.1016/j.agee.2007.11.005

Otsu N (1979) A threshold selection method from gray-level histograms. Ieee T Syst Man Cy B 1979(1):62–66. https://doi.org/10.1109/tsmc.1979.4310076

Pagliai M, Vignozzi N, Pellegrini S (2004) Soil structure and the effect of management practices. Soil till Res 79(2):131–143. https://doi.org/10.1016/j.still.2004.07.002

Pires LF, Auler AC, Roque WL, Mooney SJ (2020) X-ray microtomography analysis of soil pore structure dynamics under wetting and drying cycles. Geoderma 362:114103. https://doi.org/10.1016/j.geoderma.2019.114103

Papadopoulos A, Bird NRA, Whitmore AP, Mooney SJ (2009) Investigating the effects of organic and conventional management on soil aggregate stability using X-ray computed tomography. Eur J Soil Sci 60(3):360–368. https://doi.org/10.1111/j.1365-2389.2009.01126.x

Park EJ, Smucker AJM (2005) Saturated hydraulic conductivity and porosity within macroaggregates modified by tillage. Soil Sci Soc Am J 69(1):38–45. https://doi.org/10.2136/sssaj2005.0038

Qiao J, Liu XT, Zhu YJ, Jia XX, Shao MA (2021) Three-dimensional quantification of soil pore structure in wind-deposited loess under different vegetation types using industrial X-ray computed tomography. CATENA 199:105098. https://doi.org/10.1016/j.catena.2020.105098

Regelink IC, Stoof CR, Rousseva S, Weng L, Lair GJ, Kram P, Comans RNJ (2015) Linkages between aggregate formation, porosity and soil chemical properties. Geoderma 247:24–37. https://doi.org/10.1016/j.geoderma.2015.01.022

Rohoková M, Valla M (2011) Comparison of two methods for aggregate stability measurement-a review. Plant Soil Environ 50(8):79–382. https://doi.org/10.17221/4047-pse

Sweeting MM (1973) Karst landforms and limestones. S Afr Geogr J 55(1):8188. https://doi.org/10.1080/03736245.1973.10559518

Sarker TC, Incerti G, Spaccini R, Piccolo A, Mazzoleni S, Bonanomi G (2018) Linking organic matter chemistry with soil aggregate stability: Insight from 13 C NMR spectroscopy. Soil Biol Biochem 117:175–184. https://doi.org/10.1016/j.soilbio.2017.11.011

Six J, Paustian K (2014) Aggregate-associated soil organic matter as an ecosystem property and a measurement tool. Soil Biol Biochem 68:A4–A9. https://doi.org/10.1016/j.soilbio.2013.06.014

Schweizer SA, Bucka FB, Graf-Rosenfellner M, Kögel-Knabner I (2019) Soil microaggregate size composition and organic matter distribution as affected by clay content. Geoderma 355:113901. https://doi.org/10.1016/j.geoderma.2019.113901

Strong DT, Wever HD, Merckx R, Recous S (2004) Spatial location of carbon decomposition in the soil pore system. Eur J Soil Sci 55(4):739–750. https://doi.org/10.1111/j.1365-2389.2004.00639.x

Sexstone AJ, Revsbech NP, Parkin TB, Tiedje JM (1985) Direct measurement of oxygen profiles and denitrification rates in soil aggregates. Soil Sci Soc Am J 49(3):645–651. https://doi.org/10.2136/sssaj1985.03615995004900030024x

Smucker AJM, Wang W, Kravchenko AN, Dick WA (2010) Forms and functions of meso and micro-niches of car bon within soil aggregates. J Nematol 42(1):84–86

Tisdall JM, Oades JM (1982) Organic matter and water-stable aggregates in soils. J Soil Sci 33(2):141–163. https://doi.org/10.1111/j.1365-2389.1982.tb01755.x

White WB, White EL (2005) Ground water flux distribution between matrix, fractures, and conduits: constraints on modeling. Speleogenesis and Evolution of Karst Aquifers 3(2):2–8. https://doi.org/10.1097/00126097-200502000-00001

Wu XL, Wei YJ, Cai CF, Yuan ZJ, Li DQ, Liao YS, Deng YS (2021) Quantifying the contribution of phyllosilicate mineralogy to aggregate stability in the east Asian monsoon region. Geoderma 393:115036. https://doi.org/10.1016/j.geoderma.2021.115036

Wang MY, Xu SX, Kong C, Zhao YC, Shi XZ, Guo NJ (2019) Assessing the effects of land use change from rice to vegetable on soil structural quality using X-ray CT. Soil till Res 195:104343. https://doi.org/10.1016/j.still.2019.104343

Warner GS, Nieber JL, Moore ID, Geise RA (1989) Characterizing macropores in soil by computed tomography. Soil Sci Soc Am J 53(3):653. https://doi.org/10.2136/sssaj1989.036159950053000300

Wairiu M, Lal R (2003) Soil organic carbon in relation to cultivation and topsoil removal on sloping lands of Kolombangara. Solomon Islands Soil till Res 70(1):19–27. https://doi.org/10.1016/s0167-1987(02)00116-2

Xiao SS, Ye YY, Xiao D, Chen WR, Zhang W, Wang KL (2019) Effects of tillage on soil N availability, aggregate size, and microbial biomass in a subtropical karst region. Soil till Res 192:187–195. https://doi.org/10.1016/j.still.2019.05.006

Yu X, Fu Y, Lu S (2017) Characterization of the pore structure and cementing substances of soil aggregates by a combination of synchrotron radiation X-ray micro-computed tomography and scanning electron microscopy. Eur J Soil Sci 68(1):66–79. https://doi.org/10.1111/ejss.12399

Yang BH, Wu AX, Miao XX, Liu JZ (2014) 3D characterization and analysis of pore structure of packed ore particle beds based on computed tomography images. T Nonferr Metal Soc 24(3):833–838. https://doi.org/10.1016/S1003-6326(14)63131-9

Yu K, Duan Y, Zhang MS, Dong Y, Wang LC, Wang Y, Guo X, Hu FS (2019) Using micro focus industrial computed tomography to characterize the effects of soil type and soil depth on soil pore characteristics, morphology, and soil compression in Xi'an. China J Soil Sediment 20(4):1943–1959. https://doi.org/10.1007/s11368-019-02536-8

You Y, Wang J, Huang X, Tang Z, Liu S, Sun OJ (2014) Relating microbial community structure to functioning in forest soil organic carbon transformation and turnover. Ecol Evol 4(5):633–647. https://doi.org/10.1002/ece3.969

Yu XL, Peng GY, Lu SG (2018) Characterizing aggregate pore structure by X-ray micro-computed tomography and a network model. Soil Sci Soc Am J 82(4):744–756. https://doi.org/10.2136/sssaj2017.11.0385

Zhao Y, Hu X, Li X (2020) Analysis of the intra-aggregate pore structures in three soil types using X-ray computed tomography. CATENA 193:104622. https://doi.org/10.1016/j.catena.2020.104622

Zhou H, Peng XH, Edmund P, Xiao TQ, Peng GY (2013) Effects of organic and inorganic fertilization on soil aggregation in an Ultisol as characterized by synchrotron based X-ray micro-computed tomography. Geoderma 195–196:23–30. https://doi.org/10.1016/j.geoderma.2012.11.003

Zhou H, Peng XH, Peth S, Xiao TQ (2012) Effects of vegetation restoration on soil aggregate microstructure quantified with synchrotron-based micro-computed tomography. Soil till Res 124:17–23. https://doi.org/10.1016/j.still.2012.04.006

Zhou H, Fang H, Mooney S, Peng X (2016) Effects of long-term inorganic and organic fertilizations on the soil micro and macro structures of rice paddies. Geoderma 266:66–74. https://doi.org/10.1016/j.geoderma.2015.12.007

Zhang B, Horn R (2001) Mechanisms of aggregate stabilization in Ultisols from subtropical China. Geoderma 99(1–2):123–145. https://doi.org/10.1016/S0016-7061(00)00069-0

Zhang ZB, Zhou H, Lin H, Peng X (2016) Puddling intensity, sesquioxides, and soil organic carbon impacts on crack patterns of two paddy soils. Geoderma 262:155–164. https://doi.org/10.1016/j.geoderma.2015.08.030